Made available through Montana State University's ScholarWorks

Particle classification by image analysis improves understanding of corn stover degradation mechanisms during deconstruction

Dylan S. Cousins, Kristian P. Pedersen, William G. Otto, Asif Hasan Rony, Jeffrey A. Lacey, John E. Aston, David B. Hodge

© This manuscript version is made available under the CC-BY-NC-ND 4.0 license
https://creativecommons.org/licenses/by-nc-nd/4.0/

Particle classification by image analysis improves understanding of corn stover degradation mechanisms during deconstruction

Dylan S. Cousins[1], Kristian P. Pedersen[1], William G. Otto[1], Asif Hasan Rony[2], Jeffrey A. Lacey[2], John E. Aston[2], David B. Hodge[1,3]

1. *Department of Chemical and Biological Engineering, Montana State University, 306 Cobleigh Hall PO Box 173920 Bozeman, MT 59717-3920, USA*

2. *Idaho National* Laboratory*, Idaho Falls, ID, USA*

3. *Division of Sustainable* Process *Engineering, Luleå University of Technology, Luleå, Sweden*

*Corresponding author. *Email address*: david.hodge3@montana.edu

Abstract

Biomass feedstock heterogeneity is a principal roadblock to implementation of the biorefinery concept. Even within an identical cultivar of corn stover, different bales contain not only varying abundance moisture, ash, glucan, and other chemical compounds, but also varying abundance of tissue anatomies (e.g., leaf, husk, cob, or stalk). These different anatomical components not only differ in their response to pretreatment and enzymatic hydrolysis to glucose, but also vary in their mechanical and conveyance properties. Although this heterogeneous nature of corn stover feedstock has been identified as a challenge, a fundamental knowledge gap of how these tissues behave during biorefining processing remains. In this work, we demonstrate the use of a commercial fiber image analyzer typically used for wood fiber characterization to monitor the particle size and shapes of non-woody feedstock during milling, pretreatment, and hydrolysis. Additionally, we present novel use of Gaussian process classification to distinguish bundle, parenchyma, and fiber particles to an accuracy of 96.4%. Quantitative probability distribution plots for characteristics such as length and roundness allow elucidation of particle morphology as pretreatment and enzymatic hydrolysis progress. In both stalk pith and stalk rind, particles peel into individual cells whose walls are subsequently fragmented during enzymatic hydrolysis.

Keywords

Particle image analysis, feedstock enhancement, biomass conversion, Gaussian process classification

1. Introduction

Feedstock variability is a principal challenge to cost-competitive bioproducts (Yan et al., 2020). Recently, mechanical separation of biomass into more homogeneous streams has gained attention as a potential approach to reduce costs associated with inconsistent feedstock (Cousins et al., 2022a; Cousins et al., 2022b; Lacey et al., 2015; Thompson et al., 2016). However, the impact of such separation processes must be quantified to inform cost-effective implementation. Online and offline approaches for monitoring and/or assessing these separation processes are presently underdeveloped for non-woody plants such as corn stover that could be used in biorefining processes. This can be contrasted with wood fiber characterization/classification employed in the pulp and paper industry, where fiber characteristics of wood pulps are carefully monitored and can be correlated to the mechanical properties of the resultant paper (Kälviäinen, 2011).

Determination of particle size distributions via sieving is a mature and commonplace technique for many industrial products including among others, aggregates (Chen et al., 2005), grain (Al-Rabadi et al., 2009), and metal powders for additive manufacturing (Popovich and Sufiiarov, 2016). Particle size distributions of air-dried biomass particles from diverse sources (softwood, herbaceous dicot, and monocots) subjected to knife-milling have been investigated by sieving and were shown to have a linear cumulative mass fraction as a function of particle size (Guo et al., 2012). The same study found biomass particles to have large aspect ratios at large particle sizes, but the aspect ratio converged to 2.5 as particle size was reduced. The sieve stage to which a given particle partitions is most closely correlated to the particle's minimum Feret diameter (Altuhafi and Coop, 2011). Therefore, when comparing sieved distributions of biomass, particles with the same minimum Feret diameter will partition to the same sieve stage, but particles with high aspect ratios have been observed to be up to 17 times larger (Igathinathane et al., 2009c). Therefore, despite its simplicity and widespread use, sieve analysis does not capture subtleties in particle size distributions and a more advanced tool is needed.

Broadly speaking, the use of machine vision for biomass analysis covers a wide range of technology and application. Techniques like near-infrared (NIR) and Fourier transform infrared spectroscopy (FT-IR) can distinguish chemical composition and anatomical relative abundance (Cousins et al., 2022a; Hames et al., 2003; Templeton et al., 2009). Recently, light in the visible range has been used to characterize corn stover quality with respect to biological degradation (Ding et al., 2022). In the same work, surface characteristics were also correlated to biomass quality and ash content (Ding et al., 2022). An area that has seen comparatively less attention is the correlation of particle characteristics to feedstock quality, response to processing, and downstream yields of targeted chemicals.

Individual geometric particle characteristics have long been analyzed using machine vision across many industries including mining and aggregate (Andersson et al., 2012; Jemwa and Aldrich, 2012; Murtagh et al., 2005), agriculture (Igathinathane et al., 2008; Mavridou et al., 2019), foodstuffs (Igathinathane et al., 2009b; Patel et al., 2012) and biomass (Igathinathane et al., 2009a; Igathinathane et al., 2009c). Importantly, fiber image analysis has been commonplace in the pulp and paper industry since the 1980s to monitor pulp quality (Kälviäinen, 2011), fiber characteristics (Haapala et al., 2020), and susceptibility to enzymatic depolymerization (Mooney et al., 1999). Flow techniques wherein fibers are suspended in a liquid medium and imaged while passing through a flow-loop have been used to monitor fiber characteristics, surface chemistry, and particle swelling phenomenon (Hirn and Bauer, 2006). Modern ultra-high-definition cameras allow accurate characterization of particle fines, showing a threefold increase in the amount of area detected due to parenchyma fines (Haapala et al., 2020).

Particle size analyzers have been used to characterize the average size of biomass particles during biomass pretreatment and enzymatic hydrolysis (Chen et al., 2013; Dibble et al., 2011; Gu et al., 2018; Kapsokalyvas et al., 2018; Stickel et al., 2018). During the enzymatic hydrolysis of corn stover and wheat straw, particle size has been shown to decrease and eventually plateau and this effect was more pronounced in dilute acid pretreated biomass (Gu et al., 2018). Particle length distributions (PLDs) of corn stover determined by large-field-of-view light microscopy were found to be bimodal (Kapsokalyvas et al., 2018). The larger population of particles was shown to be length-reduced with more severe pretreatment and longer hydrolysis times shifted the PLD to the smaller population (Kapsokalyvas et al., 2018). These two studies show congruent results in shifts of particles to smaller sizes and an eventual plateau during enzymatic hydrolysis (Gu et al., 2018; Kapsokalyvas et al., 2018). Populations of small particles determined by laser diffraction were shown to increase with various refining techniques after chemical pretreatment, though a bimodal distribution persisted (Chen et al., 2013). Importantly, different sized corn stover fractions separated by sieving showed differences in protein and extractive abundance, but did not conclusively affect glucan conversion during enzymatic hydrolysis until reduced to a mesh size of #120 (125 μm) (Chundawat et al., 2007). Eucalyptus subjected to SO_2 pretreatment and subsequent H_2O_2 delignification was shown to have a rapid increase in the number of shorter particles during enzymatic hydrolysis as determined by laser scattering (Ramos et al., 1993). Use of Paper and Fiber Research Institute (PFI) mills increases the degree of fibrillation and specific surface area of wood fibers, which increases the rate of enzymatic hydrolysis, but not the final glucose yield at 53 hr (Liu et al., 2016). Generating high-throughput particle statistics ($>10^6$ particles) remains a technological barrier (Kapsokalyvas et al., 2018), but one that we show can be overcome in the present work.

Corn stover exhibits significant diversity in both chemical composition and physical properties. This heterogeneity originates from varying cell types from differing anatomical sources within the plant, and results in differences in particle responses to pretreatment and enzymatic hydrolysis (Cousins et al., 2022a; Garlock et al., 2009). Most studies regarding particle morphology of corn stover do not differentiate between different tissue classes (*e.g.*, leaf, husk, stalk, cob) or particle type (*e.g.*, parenchyma, vascular bundle, dermal tissue) (Kapsokalyvas et al., 2020; Yang et al., 2021; Zeng et al., 2007). Indeed, consideration of tissue type and particle class is important because enzyme binding has been shown to be preferential for some lignin-poor tissues within corn stover (Ding et al., 2012). For corn stover fractions sieved to varying size, liquid hot water pretreatment was shown to erase the observed differences in glucose yields that existed in untreated stover (Zeng et al., 2007).

In this work we use a commercial fiber image analyzer to quantify probability distributions of particle length, area, width, roundness, %Area, and solidity of corn stover anatomical tissues subjected to milling, alkaline pretreatment and enzymatic hydrolysis. Further, we demonstrate that these metrics can be successfully employed to classify different particle types (*e.g.*, fiber versus parenchyma), determine which particle characteristics are most pertinent to classification, and monitor the changes of particle types and their characteristics during pretreatment and enzymatic hydrolysis.

2. Materials and Methods

2.1 Biomass preparation

Corn stover used in the present study was taken from a bale harvested on October 28, 2017 in Story County, Iowa and has been described in our previous work (Cousins et al., 2022a; Cousins et al., 2022b). This corn stover was manually fractionated into sheath, leaf, stalk pith, husk, stalk rind, and cob as previously documented (Cousins et al., 2022a). After manual anatomical separation corn stover was milled to pass a #10 standard mesh (2 mm) screens using a Wiley mini-mill (Thomas Scientific, Swedesboro, NJ, USA).

2.2 Image acquisition and particle image analysis

For image analysis, approximately 50 mg of milled corn stover was suspended in 500 mL of water for analysis using an FS5 Fiber Image Analyzer (Valmet Oyj, Espoo, Finland). Samples were allowed to hydrate for approximately ten min prior to analysis. Image acquisition was conducted at a pump flow rate of 20 mL/s. Video files from the instrument were unpacked into stacks of 940 images. FIJI (Schindelin et al., 2012) was used to treat the images by enhancing the contrast of the image (saturated pixels = 0.3%), masking the image to a black background, then running the “Analyze Particles” routine, after which the outlines of particles with unique identifying numbers were kept so that they could be manually classified

(**Fig. S1**). This process returned 14 characteristics for each particle: area, perimeter, width of enclosing rectangle, height of enclosing rectangle, major axis of fitted ellipse, minor axis of fitted ellipse, angle of major axis of fitted ellipse, circularity (*circularity* = $4\pi \times (area/perimeter^2)$), Feret diameter (maximum distance calipers would achieve while rotating about the particle), minimum Feret diameter (minimum distance calipers would achieve while rotating about the particle), aspect ratio (major axis of fitted ellipse divided by minor axis of fitted ellipse), roundness (inverse of aspect ratio), solidity (**Fig. 1A, B**) and %Area, which is the amount of pixel area covered by a particle interior to its perimeter (**Fig. 1C, D, E**). In each image stack, particles are assigned unique numbers so that an operator may manually classify the particle type for a given particle to create a training dataset. Probability distributions of particle characteristics were generated by creating area-weighted histograms and the number of histogram bins (N_{bins}) is presented for each characteristic.

2.3 Manual and machine classification of particles

To build a training set, 1380 particles were manually classified by their particle type (**Fig. 2**); 611 bundle particles, 384 parenchyma particles, and 385 fiber particles were distinguished. Though manual classification is subjective to the operator, we employed heuristics to maintain as much repeatability as possible. Fibers are identified by high aspect ratio, narrow width, and tendency to have kinks or bends. Bundles are generally larger, lower aspect ratio particles with angular edges and consist of fibrous material that has not been broken apart. Parenchyma particles are easily distinguished by their porous structure. For classification, particles that had an overall area less than 3,000 μm^2 were classified as fines and omitted from subsequent analysis.

Using this dataset of 1380 manually classified particles, we implemented various classification algorithms to test their efficacy at determining particle type (fiber, bundle, or parenchyma). A subset of the 1380 particles was taken in which 384 particles of each type were used for model training. In this way, particle types are not overrepresented in predictions due to greater abundance in the training data set. As a first pass screening test, ten classification algorithms were implemented from scikit-learn (version 0.24.2): known nearest neighbors, linear support vector machine (L-SVM), radial basis function (RBF) support vector machine (SVM), Gaussian process (GP), decision tree, random forest, neural network (NN), adaptive boosting, naïve Bayes, and quadratic discriminant analysis (QDA) (Pedregosa et al., 2011). Principal component analysis (PCA) was used to visualize grouping of particle types by loadings of the first three principal components. Subsequent classification of particles was conducted using GP. GP classification attempts to approximate a function and use it to map predictor variables (in this case, particle features) onto a class (in this case, particle type) (Nickisch and Rasmussen, 2008). The code for

classifier comparison, PCA, and particle distribution plotting after training can be accessed in the Supporting Information.

2.4 Composition analysis, pretreatment, and enzymatic hydrolysis

Composition analysis of structural polysaccharides, lignin, and ash content was conducted according to laboratory analysis procedures developed by the National Renewable Energy Laboratory (Sluiter et al., 2012; Sluiter and Sluiter, 2011).

Anatomically pure samples of stalk rind and stalk pith were subjected to aqueous alkaline pretreatment at a 10% solids (w/v) loading with 10% sodium hydroxide (w/w) with 3 g of dry biomass. Pretreatment was conducted in a 40 mL Teflon reaction vessel held shut in a stainless-steel housing. After thoroughly mixing the reactants, they were loaded in the reactor and placed in a 90 ˚C sand bath. The temperature of the sand bath decreased upon insertion of the reactor units and was monitored until it reached steady-state at 90 ˚C. From this point, the pretreatment was allowed to proceed for 1 hr after which the reactors were removed and submerged in 10 ˚C water for ten min. The biomass was then removed from the reactor, rinsed with approximately 250 mL of DI water, then pH adjusted in 500 mL of water using 6M sulfuric acid to achieve a pH of 4.9. The biomass was then vacuum filtered from the water and stored in a sealable polyethylene bag in a 4 ˚C refrigerator until use for enzymatic hydrolysis, which occurred no more than 24 hr after pretreatment.

Conditions for enzymatic hydrolysis of anatomical fractions of corn stover have also been described in our previous work (Cousins et al., 2022a). Briefly, enzymatic hydrolysis was carried out on pretreated stalk pith and stalk rind. The hydrolysis vessels were 15-mL centrifuge tubes at 10 % (wt/liquid vol) solids loading with 15 mg Cellic CTec2 (SAE0020 Sigma-Aldrich) enzyme per g of glucan buffered using a 50 mM sodium citrate buffer (pH 5) in a rotating incubator (198° of rotation) at 60 rpm at 50 °C.

For timed enzymatic hydrolysis, ten hydrolysis tubes were initially prepared for each tissue type. The hydrolysis was terminated at 30 min, 1 hr, 6 hr, 12 hr, and 72 hr for replicate tubes by 5x dilution of the sample, from which aliquots were taken for HPLC measurement for saccharide quantification. Samples were then immediately image analyzed by diluting them in approximately 500 mL of tap water. Glucose yield from enzymatic hydrolysis was determined by diluting the hydrolysis liquor ten-fold and measuring saccharide and acetate concentration on an Agilent 1260 series HPLC equipped with an Aminex HPX-87H column (Bio-Rad, Hercules, CA, USA) using 5 mM aqueous H_2SO_4 as the mobile phase coupled with RI detection. Hydrolysis yields are given in terms of percent of maximum theoretical glucose produced based on the quantified cellulose content in the pretreated biomass.

2.5 Confocal microscopy

Micrographs of a transverse section of corn stalk were generated using a Leica SP8 Confocal Scanning Laser Microscope (Leica, Wetzlar, Germany) using a HC PL APO CS2 10x/0.40 DRY objective. The 405 nm excitation line was used to generate autofluorescence from lignin present in the samples. The detector collected wavelengths from 425nm to 673nm.

3. Results and discussion

3.1 Particle feature distributions

Particle feature distributions can inform processing because particles from various anatomical tissues have different distributions for a given milling size. For example, the aspect ratio of particles can greatly affect the pneumatic (Hilton and Cleary, 2011) and mechanical (Govender et al., 2021) conveyance of particles and slurry rheology (Djalili-Moghaddam and Toll, 2006; Gunes et al., 2008). Moreover, milling size has been shown to be correlated to enzymatic hydrolysis yields due to an increased surface-area-to-volume ratio (Chundawat et al., 2007; Dasari and Eric Berson, 2007). Therefore, tissues that reliably mill to smaller sizes could be targeted for enzymatic hydrolysis. However, tissues do not consistently mill to a defined sieve size. For example, cob and leaf show different length distributions at a 2-mm screen size (**Fig. 3A**). Leaf has a bimodal distribution while cob particles are observed to be monomodal. Cob particles that are milled to pass a 0.85-mm screen are observed to shift to lower lengths. Leaves maintain some longer particles but the population of larger particles at a 2-mm screen size is observed to transition to the population of smaller particles at a 0.85-mm screen size. Leaves are delicate tissues and are easily pulverized during handling of corn stover (Emerson, 2020) so the smaller of the two populations of the 2-mm screen sample may be inherent to the bale. Conversely, cob is more mechanically robust so its particle distribution responds more predictably to the mesh size (*i.e.*, a smaller screen produces a smaller monomodal distribution). Components of the stalk (pith and rind) show a less-pronounced bimodal distribution at a 2-mm screen size with more of the particles populating the peak that occurs around 0.1 mm (**Fig. 3B**). The peak that occurs at 1 mm for pith at the 2-mm screen size is greatly diminished at the 0.85 mm screen size. Furthermore, larger particles that occur in rind at the 2-mm screen size are greatly diminished when this tissue is milled to pass a 0.85-mm screen.

A distinct advantage of particle image analysis compared to a technique such as sieving is the ability to calculate other particle shape descriptors beside sieve diameter (Igathinathane et al., 2009c). For example, particles from different components of the stalk (pith and rind) display a distinct difference in roundness (the inverse of aspect ratio) (**Fig. 4A**). Generally, neither rind nor pith particles display a significant change in roundness at the two milling sizes. Percent area (%Area) of a given particle is the area of the

masked particle divided by the total area that is encompassed by its perimeter (**Fig. 1C-E**). Parenchyma is spongy tissue that often retains multiple lumen of multiple adjacent cells that contribute to a lower %Area compared to fibrous particles. Since stalk pith is enriched in parenchyma, it displays distributions of particles that have lower %Area than those of the rind, which is enriched in fibrous epidermal cells (**Fig. 4B**). These results demonstrate the utility of the instrument and analysis technique to describe particle features of milled corn stover. Non-standard shape descriptor metrics such as %Area can be useful to gain insight into the relative abundance of certain particle types and how these particles behave during chemical pretreatments and enzymatic hydrolysis.

3.2 Particle classification by image analysis

Sets of particles were visually classified based on their characteristics into three classes (bundle, parenchyma, and fiber) and used to train and validate classification models. These particle types are of particular interest because of their demonstrated (Cousins et al., 2022a) differing response to mild alkaline pretreatment and enzymatic hydrolysis and they are generally able to be distinguished from one another. The present study aims to demonstrate the difference in morphology between these particle types during processing. Of the ten classification algorithms tested here, six have accuracy greater than 90% over the 30 repeat model evaluations (**Table 1**). An example of confusion matrices generated during a single training/test split is presented in **Fig. S2**. In these cases, the greatest confusion occurs between bundle and parenchyma, which have more similar characteristics (*e.g.*, aspect ratio) compared to fibers. Gaussian process classification is observed to have the highest average classification accuracy and best repeatability, so we used this technique for particle classification in the remaining work.

To better understand the characteristics that are associated with particle types, a correlation matrix was generated for the data used for particle classification (**Fig. 5**). Generally, differences in correlation between characteristics allow more fidelity in the distinction of particle types. For example, roundness has a strong negative correlation with fiber and a strong positive correlation with parenchyma, so it provides a robust indicator to distinguish between these particle types. Bundles are observed to have relatively weak correlations to the particle characteristics compared to the other two particle types with the strongest Pearson correlation coefficient equal to 0.43 (solidity). Generally, the characteristics that are correlated to bundles have the opposite correlations to fibers. The confusion in prediction generally comes from distinguishing between bundles and parenchyma, whereas fibers are rarely misclassified (**Fig. S2**). Even though these two particle types have less distinction between their correlations to particle characteristics compared to fibers, most classifier algorithms are still able to distinguish these two particle types to reasonable accuracy (**Fig. S2**).

Particle characteristics are themselves correlated (*e.g.*, minimum Feret diameter and minor axis), so it is informative to conduct PCA to discern how much of the variance in the predictors (particle characteristics) can be explained by orthogonal linear combinations. Indeed, 99.6% of the variance is explained by the first three principal components (**Fig. 6A**). Much of the distinction between these particles can be made from three particle characteristics: %Area, aspect ratio, and perimeter (**Fig. 6B**). PC1 has strong loadings for aspect ratio and %Area so can distinguish between bundle or fiber and parenchyma. PC2 also has a strong loading in aspect ratio, but has a strong negative loading in %Area that leads to better distinction between parenchyma and bundles. PC3 has a strong loading for perimeter that allows bundles, which are generally larger, to be distinguished from the other two particle types.

3.3 Classification informs morphological changes during enzymatic hydrolysis

Confocal micrographs with lignin autofluorescence taken of a transverse section of corn stalk show the anatomical features that frame the discussion of the development of corn stover particles and their morphological changes during processing (**Fig. 7**). Stalk pith includes everything interior to the epidermis of the stalk, including vascular bundles and parenchyma, and stalk rind is the epidermis tissue. Parenchyma cells (**Fig. 7A**, Pa) tend to be less lignified with large intercellular space. The appearance of dual walls is an artifact of the projection of the z-stack of images onto a single image. Unlike parenchyma, cells that comprise the vascular bundle (**Fig. 7A**, Va) have heavily lignified secondary cell walls. The rind cells, sclerenchyma (**Fig. 7B**, Sc) and epidermis (**Fig. 7B**, Ep), are also observed to fluoresce heavily suggesting a high abundance of lignin in their cell walls. Because these images are taken transverse to the long axis of the corn stalk, the high aspect ratio of the cells of the vascular bundle and epidermis is not captured. The goal of the work presented in this section is to monitor the size and shape characteristics of particles composed of these various cell types during alkaline pretreatment and enzymatic hydrolysis.

In this section, we report the utility of particle imaging and classification to monitor pretreatment and enzymatic hydrolysis of stalk components. We chose to investigate the pith and rind components of the stalk due to 1) their different chemical composition and 2) stalks can be effectively isolated as an independent stream in a mechanical separation process (Cousins et al., 2022a; Cousins et al., 2022b). The components of stalk show different susceptibility to enzymatic hydrolysis on both raw and pretreated material (Cousins et al., 2022a). Therefore, we subjected manually fractionated stalk rind and pith to mild alkaline pretreatment (100 mg NaOH/g biomass, 1 hr, 90 ˚C). Enzymatic hydrolysis was carried out and stopped at varying times to determine glucose yields and to measure particle characteristics with the image analyzer. As expected, glucose yields (as % of theoretical maximum) show that pith is less recalcitrant to hydrolysis compared to stalk rind (**Fig. 8**), commensurate with our previous results

(Cousins et al., 2022a). The following sections describe the changes in particle characteristics for stalk pith and stalk rind during alkaline pretreatment and subsequent enzymatic hydrolysis, focusing on the early (30 min to 12 hr) and latter (12 hr to 72 hr) stages of hydrolysis.

3.3.1 Morphological changes during pretreatment

Inspection of exemplary raw images of chemical pretreatment and progressive enzymatic hydrolysis of pith (**Fig. 9**) and rind (**Fig. 10**) allows a qualitative description of the changes of particle types during these processes. A noteworthy occurrence is the disappearance of fines after pretreatment for both pith and rind. Alkaline pretreatment preferentially solubilizes lignin (Karp et al., 2014) but it is unlikely that the majority of the initial fine particles in the biomass are composed predominantly of lignin. More probably, the disappearance of fine particles is due to the filtration step during biomass recovery after pretreatment; very fine particles are likely able to pass through the #200 mesh (0.075 mm) used for filtration. Indeed, image analysis confirms a reduction in the relative abundance of fines (defined as particles with area less than 0.003 mm^2) after the pretreatment step for both pith and rind (**Fig. S3**).

After pretreatment, pith particle lengths are shown to increase for those particles classified as bundles, remain the same for particles classified as fibers, and decrease for particles classified as parenchyma (**Fig. 11**). The peak of the length distribution for bundle particles increases from approximately 0.4 mm to approximately 2 mm. Manual inspection of images suggests that particles do not have such a drastic increase in length, so this increase must be due to bundles splitting axially, thereby creating more particles that contribute to a greater total area of observed bundles. Unexpectedly, particle classification shows that parenchyma particles only account for 28% of the total particle area for raw pith (**Fig. S4A**) and only 12% of the area after pretreatment. Indeed, many of the larger particles, which account for a substantial portion of the total particle area after pretreatment, appear to be vascular bundles to which some parenchyma cells are still attached (**Fig. 9B**, blue upward-facing arrow). An interesting finding is that aggregates of parenchyma particles are observed to be in the process peeling following pretreatment (**Fig. 9B**, green right-facing arrow). Such peeling yields high aspect ratio "rods" of parenchyma particles (**Fig. 9B**, red left-facing arrow). The presence of many of these high aspect ratio rods suggests a preferential degradation of parenchyma cells along their cell walls that are oriented parallel to the axial direction of the stalk. Such rods likely contribute to the observed decrease in roundness of all pith particles types during pretreatment (**Fig. 12**). Solidity is also shown to decrease during pretreatment for all pith particle types except for fibers (**Fig. S5**) suggesting that more protuberances from bundle particles are present after pretreatment, lending further evidence to the proposed peeling mechanism of particle degradation. Such fragmentation and peeling have also been observed in pretreated softwood and hardwood (Arantes et al., 2014) and fibrillation degree is highly correlated to enzymatic hydrolysis yields (Liu et al., 2016).

New particle area created due to splitting of particles, as described above, can cause misinterpretation of the origin of the shift in particle length distribution. The shift to longer (**Fig. 11C**) and larger (**Fig. S6C**) particles could alternatively be interpreted as swelling of parenchyma cells during alkaline pretreatment. Disruption of the cell wall matrix from lignin removal leads to increased access for water and has a swelling effect (Williams and Hodge, 2014). A measure of particle characteristic that is uncorrelated to size can provides a clearer description of the effect of pretreatment. %Area is one such shape descriptor; it measures the amount of pixel area covered by a particle interior to its perimeter (**Fig. 11C-E**). One of the defining characteristics of parenchyma is that is tends to have lower %Area than other particle types (**Fig. 5**). The distribution of %Area increases (*i.e.*, a decrease in void area) for bundle and parenchyma particles in pith during alkaline pretreatment (**Fig. S7B, C**) and is likely due to lignin removal and swelling of the cell wall, which tends to "crowd" the parenchyma intracellular space (Liao et al., 2022; Williams and Hodge, 2014).

Interestingly, the opposite effect is observed for stalk rind during pretreatment in which an overall decrease in %Area (*i.e.*, an increase in void area) occurs (**Fig. S8**). This finding is corroborated by the fact that the particles classified as "fiber" in the pith fraction also see an overall decrease in %Area after pretreatment (**Fig. S7D**). Previously, we have shown that the stalk rind contains a higher abundance of lignin compared to stalk pith (Cousins et al., 2022a). Vascular bundles and their associated sclerenchyma within the stalk pith are also shown to be more lignified compared to the surrounding parenchyma both here (**Fig. 7B**) and in other work (Liao et al., 2022). The differing effects of alkaline pretreatment on the %Area of parenchyma and fibrous tissues can likely be attributed to the relative difference in lignin removal from the tissues. In parenchyma, the lack of lignified primary cell walls may cause them to easily swell and decrease the observed void area. Conversely, in epidermal cells, sclerenchyma, and vascular bundles, the high abundance of lignin, when removed during pretreatment, likely causes fibrillation of the cells and more observed void area. In a similar phenomenon to pith particles, rind particles are observed to increase in length and area after pretreatment (**Fig. 13**, **Fig. S9**). In an analogous mechanism to pith, this is likely due to splitting of bundle particles to create more observed area at large particle sizes. Solidity and %Area also decrease for pretreated rind particles suggesting a shift toward more perturbed and enzyme-accessible particle morphologies.

3.3.2 Morphological changes during early stages of enzymatic hydrolysis (30 min to 12 hr)

Between 30 min and 6 hr, the fines content observed in stalk pith increases only slightly (**Fig. S3**). During this time, changes in particle morphology are largely attributable to dissociation of parenchyma aggregates into individual cells. After only 30 min of enzymatic hydrolysis, many parenchyma cells are observed as individual particles (**Fig. 9C**, red left-facing arrow). Correspondingly, the particle length

distribution of pith bundles also shows a drastic decrease after only 30 min of enzymatic hydrolysis (**Fig. 11B**). This suggests a cleavage of parenchyma cell walls in the plane orthogonal to the long axis of the rods. Interestingly, particles classified as parenchyma show an increase in particle length between pretreated and 30 min hydrolyzed tissues (**Fig. 11C**). We conjecture that this is due to an overall increase in parenchyma area due to individual parenchyma cells being cleaved from bundles in the first 30 min of hydrolysis, where mostly fine particles had been classified as parenchyma after pretreatment, rather than an increase in particle size. This conjecture is supported by the increase in the overall percentage of area that is classified as parenchyma between pretreatment and 30 min of enzymatic hydrolysis (**Fig. S4A**).

As enzymatic hydrolysis proceeds, pith particles display a decrease in %Area distribution for parenchyma particles, but a slight increase for bundles. During this time, the appearance of low %Area individual parenchyma cells (**Fig. 9C**, red left-facing arrow) likely explains this decrease. After 6 hr, such cells are less prevalent; the rate of cell wall fragmentation has overtaken the rate of individual cell formation. This observation is confirmed by the increase in the probability distribution of %Area (**Fig. S7C**). That is, cell wall fragments will have a high %Area (low void area) because they have no enclosed space, whereas whole parenchyma cells will have a low %Area (high void area). Solidity of pith parenchyma increases slightly during the first 30 min of hydrolysis where a new peak is observed around 0.95 (**Fig. S5C**). We propose that this peak is due to the formation of individual cells that have relatively high solidity. Pith roundness is only observed to change meaningfully in the first 6 hr of enzymatic hydrolysis for bundle particles, which show a shift to higher aspect ratio particles. This could be due to 1) increase in aspect ratio of bundles as more parenchyma "rods" are cleaved from their surfaces and/or 2) such "rods", which have low roundness, being classified as bundles. Due to the low %Area of the rods and the likelihood that they are classified as parenchyma, we suggest that the reduction in roundness of pith bundles at 6 hr is primarily due to the former conjecture.

Between 30 min and 6 hr, the fines content observed in stalk rind increases more rapidly compared to pith (**Fig. S3**). It is likely that not only are fibrous bundles breaking into individual fibrous cells, which are bigger than the fines threshold (fines < 0.003 mm^2), but that these cells further break down into fragments. During the early stages of enzymatic hydrolysis of stalk rind, the fiber length probability distribution shifts to *longer* particles (**Fig. 13D**) and a bimodal distribution is observed. Other authors have also observed the presence of bimodal distributions for corn stover during enzymatic hydrolysis (Kapsokalyvas et al., 2018), though the number and size of large particles in that study may be overestimated due to flocculation of small particles on microscope slides. In this way, *the fiber image analyzer offers a distinct technological advantage over previous analytical techniques*. The observation of a bimodal distribution in the present work is due to an increase in longer fibers (**Fig. 10C**, green right-

facing arrow) that peel off bundle particles (**Fig. 10C**, red left-facing arrow) in the first 12 hr of enzymatic hydrolysis, combined with to the predominantly short fibers that are present due to milling before hydrolysis begins. This important fibrillation effect is observed to begin within 30 min of the start of enzymatic hydrolysis and the longer peak of the bimodal distribution increases through 12 hr (**Fig. 13D**). The growth of this peak indicates that the rate of fibrillation must outweigh the rate of degradation of individual fibrous cells into shorter fragments. Nevertheless, the increase in fines during the first 12 hr (**Fig. S3**) does suggest that these fibers are further broken down into fragments. These coupled observations suggest relatively quick enzymatic activity on the primary cell walls of epidermal, sclerenchyma, and bundle sheath cells, with comparatively slower activity on the secondary cell walls. Other work using image analysis has also observed an increase followed by a decrease of intermediate-length (0.5 to 2.5 mm) flax fibers during combined mechanical treatment and enzymatic hydrolysis (Digaitis et al., 2019).

The fibrous particles in stalk pith are vascular bundles that are more easily pulverized than the epidermal tissues found in stalk rind. Indeed, the area of fibrous particles found in pith have a distribution that is shifted to smaller particles (**Fig. S6D**) compared to those of rind (**Fig. S9D**). A similar trend is observed for particle length, but the difference in length of fibrous particles in pith and rind is less pronounced than it is for area. Bundle particles for both pith and rind tend towards smaller particles as hydrolysis proceeds, but a population of larger particles is observed to persist through about 12 hr for both tissue types (**Figs. S6B** and **S9B**). These persistent bundles are likely epidermal, vascular, and sclerenchyma cells that are more lignified to start.

Interestingly, the width of fiber particles is roughly the same for pith and rind (distribution centered around 0.03 mm) and does not change appreciably with pretreatment or hydrolysis (**Figs. S10D** and **S11D**). This suggests that the vascular bundle and surrounding sclerenchyma cells have a similar diameter to the cells of the epidermis (Himmel, 2008), which is confirmed in confocal micrographs (**Fig. 7**). As individual cells peel away from larger bundles during enzymatic hydrolysis of the primary cell walls, the resultant fibrous cells persist at the same width. However, reduction in the fiber length is observed as enzymatic hydrolysis proceeds and may even lead to shorter fiber particles being "reclassified" as bundles due to lower aspect ratio. In contrast to pith, the roundness of parenchyma particles in rind decreases quickly, but then levels off for the remainder of hydrolysis (**Fig. 14C**). This may be attributable to smaller particles being classified as parenchyma in this case. Other rind tissues are also observed to decrease in roundness, likely due to the increase in high aspect ratio fibers being cleaved from the rind bundles, both of which will manifest as a decrease in observed particle roundness. %Area is observed to decrease for parenchyma particles of stalk rind as enzymatic hydrolysis proceeds due to degradation of the structure of

these cell types (**Fig. S8C**). Parenchyma is the only particle class with meaningful representation of %Area, as expected, since most fibers and bundles of rind are completely filled.

3.3.3 Morphological changes during later stages of enzymatic hydrolysis (12 hr to 72 hr)

As enzymatic hydrolysis proceeds to 72 hr for stalk pith, bundle particles continue to decrease in length (**Fig. 11B**) and area (**Fig. S6B**). Negligible changes in size metrics are observed for parenchyma particles at this point, likely because they are predominantly fines by 12 hr. Similarly, %Area shows marginal change as the last of the cells are degraded over the latter stages of enzymatic hydrolysis (**Fig. S7**). Changes in rind morphology during this time follow a similar trend with particles shifting towards smaller size metrics such as length, area and width (**Fig. 13**, **Fig S9**, and **Fig. S11**). Of note is that rind fibers, like those in pith, are shown to be reduced in length due to the high aspect ratio cells being broken in a transverse direction to their longest axis (**Fig. 13D**).

Parenchyma particles of pith tend towards higher aspect ratios (lower roundness) at longer enzymatic hydrolysis times (**Fig. 12C**). This is likely due to small fragments being classified as parenchyma and has little meaningful explanation for the particle morphology as hydrolysis proceeds. Indeed, the same trend is observed for all pith particles; as larger, round structures in pith are broken down into individual fragments, the overall roundness of the particles tends to decrease.

3.4 Discussion

Particle morphology of the stalk components during pretreatment and enzymatic hydrolysis changes in a quantifiable way as measured by particle image analysis using a commercial fiber image analyzer. Parenchyma bundles are shown to split into rod-shaped particles during pretreatment and then quickly into individual cells during enzymatic hydrolysis. Fibrous bundles prevalent in the stalk rind show fibrillation into individual cells during the initial stages of enzymatic hydrolysis and these individual fibrous cells are degraded into fragments by 72 hr. Classification allows for an important distinction between particle types that allows greater insight into the mechanisms of degradation and associated morphological changes that have not hitherto been described in the literature. Observed morphological changes have important rheological and rheokinetic implications for the processing of biomass, but most studies to date only consider an equivalent diameter or sieve size as a geometric parameter (Dibble et al., 2011; Stickel et al., 2018; Viamajala et al., 2009). Future rheological studies should combine multiple particle geometric characteristics, like those described herein, with hygroscopicity data such as water retention value (Williams et al., 2017) and pore accessibility parameters as determined with NMR (Ishizawa et al., 2007). %Area is a parameter that should be evaluated for correlation with hydrolysis yield over a wider range of corn stover tissues types since varying tissues are shown to have different

yields (Cousins et al., 2022a). Importantly, fiber attrition has been shown to vary under different pretreatments for the same mechanical mixing scheme, and vice versa (Digaitis et al., 2021). These effects should be investigated in the context of particle classification (*i.e.*, for parenchyma versus fiber particles).

The glucose yield of stalk pith during enzymatic hydrolysis at 12 hr (80%) are greater than for stalk rind at 72 hr (75%). These findings suggest that fractionation of corn stalk into its anatomical constituents of pith and rind can enable higher throughput by decreasing the residence time for a significant amount of biomass. Physical fractionation techniques that enable such separations and the effects of downstream processing on the resultant fractions should be investigated in future work.

4. Conclusions

In this work, we demonstrate the use of a commercial fiber image analyzer to monitor the morphological characteristics of corn stover particles during milling, alkaline pretreatment, and enzymatic hydrolysis over time. Additionally, we present a novel use of Gaussian process classification to distinguish between bundles, parenchyma, and fiber particles. We show that certain particle characteristics are strongly positively or negatively correlated with particle types (*e.g.*, %Area with parenchyma). Plotting loadings of the first three principal components from PCA gives an intuitive visual representation of how a classifier can distinguish between these particle types. Such classification allows greater insight into the mechanisms of degradation during pretreatment and hydrolysis; change of probability distributions of particle length, area, width, roundness, %Area and solidity show that fibrous bundles and aggregates of parenchyma split into fibers or rod-like structures during pretreatment and the early stages of enzymatic hydrolysis, respectively. This initial splitting is followed by degradation of these high aspect ratio particles in the transverse direction and finally, cell walls are broken down into individual fine fragments. Future work should explore the ability to use this tool to quantify the amount of parenchyma cells over a greater range of corn stover tissues (*e.g.*, husk and cob) and further correlate the relative abundance of particle type to glucose yields from enzymatic hydrolysis. The approaches used here, or similar advancements in characterizing feedstock particles, are a necessary development to improve, and better understand, the cost benefits of both existing and potential feedstock preprocessing and pretreatment unit operations in the bioenergy economy.

Acknowledgements

The authors would like to thank Dr. Barkan Sidar for his assistance with confocal microscopy and interpretation of the micrographs.

Funding

This material is based upon work supported by the U.S. Department of Energy's Office of Energy Efficiency and Renewable Energy (EERE) Bioenergy Technologies Office (BETO) and FOA-0002029 under the Award Number DE-EE0008907 "Enhanced Feedstock Characterization and Modeling to Facilitate Optimal Preprocessing and Deconstruction of Corn Stover".

References

Al-Rabadi, G.J.S., Gilbert, R.G., Gidley, M.J., 2009. Effect of particle size on kinetics of starch digestion in milled barley and sorghum grains by porcine alpha-amylase. J. Cereal Sci. 50, 198-204. https://doi.org/10.1016/j.jcs.2009.05.001

Altuhafi, F.N., Coop, M.R., 2011. Changes to particle characteristics associated with the compression of sands. Géotechnique 61, 459-471. https://doi.org/10.1680/geot.9.P.114

Andersson, T., Thurley, M.J., Carlson, J.E., 2012. A machine vision system for estimation of size distributions by weight of limestone particles. Minerals Eng. 25, 38-46. https://doi.org/10.1016/j.mineng.2011.10.001

Arantes, V., Gourlay, K., Saddler, J.N., 2014. The enzymatic hydrolysis of pretreated pulp fibers predominantly involves "peeling/erosion" modes of action. Biotechnol. Biofuels 7, 87. https://doi.org/10.1186/1754-6834-7-87

Chen, J.-S., Chang, M.K., Lin, K.Y., 2005. Influence of coarse aggregate shape on the strength of asphalt concrete mixtures. J. Eastern Asia Soc. Trans. Stud. 6, 1062-1075. https://doi.org/10.11175/easts.6.1062

Chen, X., Kuhn, E., Wang, W., Park, S., Flanegan, K., Trass, O., Tenlep, L., Tao, L., Tucker, M., 2013. Comparison of different mechanical refining technologies on the enzymatic digestibility of low severity acid pretreated corn stover. Bioresour. Technol. 147, 401-408. https://doi.org/10.1016/j.biortech.2013.07.109

Chundawat, S.P.S., Venkatesh, B., Dale, B.E., 2007. Effect of particle size based separation of milled corn stover on AFEX pretreatment and enzymatic digestibility. Biotechnol. Bioeng. 96, 219-231. https://doi.org/10.1002/bit.21132

Cousins, D.S., Otto, W.G., Rony, A.H., Pedersen, K.P., Aston, J.E., Hodge, D.B., 2022a. Near-Infrared Spectroscopy can Predict Anatomical Abundance in Corn Stover. Front. Energ. Res. 10. https://doi.org/10.3389/fenrg.2022.836690

Cousins, D.S., Rony, A.H., Otto, W.G., Pedersen, K.P., Hernandez, S., Lacey, J.A., Aston, J.E., Hodge, D.B., 2022b. Predictive models enhance feedstock quality of corn stover via air classification. Biomass Conv. Biorefin. https://doi.org/10.1007/s13399-022-03307-1

Dasari, R.K., Eric Berson, R., 2007. The effect of particle size on hydrolysis reaction rates and rheological properties in cellulosic slurries. Appl. Biochem. and Biotechnol. 137, 289-299. https://doi.org/10.1007/s12010-007-9059-x

Dibble, C.J., Shatova, T.A., Jorgenson, J.L., Stickel, J.J., 2011. Particle morphology characterization and manipulation in biomass slurries and the effect on rheological properties and enzymatic conversion. Biotechnol. Prog. 27, 1751-1759. https://doi.org/10.1002/btpr.669

Digaitis, R., Thybring, E.E., Thygesen, L.G., 2019. Investigating the role of mechanics in lignocellulosic biomass degradation during hydrolysis. Biotechnol Prog. 35, e2754. https://doi.org/10.1002/btpr.2754

Digaitis, R., Thybring, E.E., Thygesen, L.G., 2021. Investigating the role of mechanics in lignocellulosic biomass degradation during hydrolysis: Part II. Biotechnol Prog. 37, e3083. https://doi.org/10.1002/btpr.3083

Ding, L., Hoover, A.N., Emerson, R.M., Lin, K.-T., Gruber, J.N., Donohoe, B.S., Klinger, J.L., Colby, R.D., Thomas, B.J., Smith, W.A., Ray, A.E., 2022. Image Analysis for Rapid Assessment and Quality-Based Sorting of Corn Stover. Front. Energ. Res. 10. https://doi.org/10.3389/fenrg.2022.83769

Ding, S.-Y., Liu, Y.-S., Zeng, Y., Himmel Michael, E., Baker John, O., Bayer Edward, A., 2012. How Does Plant Cell Wall Nanoscale Architecture Correlate with Enzymatic Digestibility? Science 338, 1055-1060. https://doi.org/10.1126/science.1227491

Djalili-Moghaddam, M., Toll, S., 2006. Fibre suspension rheology: effect of concentration, aspect ratio and fibre size. Rheolog. Acta 45, 315-320. https://doi.org/10.1007/s00397-005-0021-y

Emerson, R.M., 2020. Data Qualification Framework, Leveraging Existing Bioenergy Data Workshop, Virtual. INL/CON-20-58997-Revision-0. July 2020. https://www.osti.gov/servlets/purl/1668770.

Garlock, R.J., Chundawat, S.P.S., Balan, V., Dale, B.E., 2009. Optimizing harvest of corn stover fractions based on overall sugar yields following ammonia fiber expansion pretreatment and enzymatic hydrolysis. Biotechnol. Biofuels 2, 29. https://doi.org/10.1186/1754-6834-2-29

Govender, N., Cleary, P.W., Wilke, D.N., Khinast, J., 2021. The influence of faceted particle shapes on material dynamics in screw conveying. Chem. Eng. Sci. 243, 116654. https://doi.org/10.1016/j.ces.2021.116654

Gu, H., An, R., Bao, J., 2018. Pretreatment refining leads to constant particle size distribution of lignocellulose biomass in enzymatic hydrolysis. Chem. Eng. J. 352, 198-205. https://doi.org/10.1016/j.cej.2018.06.145

Gunes, D.Z., Scirocco, R., Mewis, J., Vermant, J., 2008. Flow-induced orientation of non-spherical particles: Effect of aspect ratio and medium rheology. J. Non-Newtonian Fluid Mech. 155, 39-50. https://doi.org/10.1016/j.jnnfm.2008.05.003

Guo, Q., Chen, X., Liu, H., 2012. Experimental research on shape and size distribution of biomass particle. Fuel 94, 551-555. https://doi.org/10.1016/j.fuel.2011.11.041

Haapala, A., Riippa, T., Niskanen, T., 2020. Valmet FS5 upgraded to UHD image quality: new opportunities for lab analysis of fibres, fines and fibrils. Appita Mag., 55-61. https://doi.org/10.3316/informit.485016260477398

Hames, B.R., Thomas, S.R., Sluiter, A.D., Roth, C.J., Templeton, D.W., 2003. Rapid biomass analysis. Appl. Biochem. Biotechnol. 105, 5-16. https://doi.org/10.1385/ABAB:105:1-3:5

Hilton, J.E., Cleary, P.W., 2011. The influence of particle shape on flow modes in pneumatic conveying. Cehm. Eng. Sci. 66, 231-240. https://doi.org/10.1016/j.ces.2010.09.034

Himmel, M.E. (Ed.), 2008. Biomass Recalcitrance: Deconstructing the Plant Cell Wall for Bioenergy. Blackwell Publishing Ltd.

Hirn, U., Bauer, W., 2006. A review of image analysis based methods to evaluate fiber properties. Lenzinger Berichte 86, 96-105. https://online.tugraz.at/tug_online/voe_main2.getvolltext?pcurrpk=27320

Igathinathane, C., Melin, S., Sokhansanj, S., Bi, X., Lim, C.J., Pordesimo, L.O., Columbus, E.P., 2009a. Machine vision based particle size and size distribution determination of airborne dust particles of wood and bark pellets. Powder Technol. 196, 202-212. https://doi.org/10.1016/j.powtec.2009.07.024

Igathinathane, C., Pordesimo, L.O., Batchelor, W.D., 2009b. Major orthogonal dimensions measurement of food grains by machine vision using ImageJ. Food Res. Inter. 42, 76-84. https://doi.org/10.1016/j.foodres.2008.08.013

Igathinathane, C., Pordesimo, L.O., Columbus, E.P., Batchelor, W.D., Methuku, S.R., 2008. Shape identification and particles size distribution from basic shape parameters using ImageJ. Comp. Elect. Ag. 63, 168-182. https://doi.org/10.1016/j.compag.2008.02.007

Igathinathane, C., Pordesimo, L.O., Columbus, E.P., Batchelor, W.D., Sokhansanj, S., 2009c. Sieveless particle size distribution analysis of particulate materials through computer vision. Comp. Elect. Ag. 66, 147-158. https://doi.org/10.1016/j.compag.2009.01.005

Ishizawa, C.I., Davis, M.F., Schell, D.F., Johnson, D.K., 2007. Porosity and Its Effect on the Digestibility of Dilute Sulfuric Acid Pretreated Corn Stover. J. Agric. Food Chem. 55, 2575-2581. https://doi.org/10.1021/jf062131a

Jemwa, G.T., Aldrich, C., 2012. Estimating size fraction categories of coal particles on conveyor belts using image texture modeling methods. Expert Sys. Appl. 39, 7947-7960. https://doi.org/10.1016/j.eswa.2012.01.104

Kälviäinen, H., 2011. Machine vision based quality control from pulping to papermaking for printing. Pattern Recog. Image Anal. 21, 486. https://doi.org/10.1134/S1054661811020441

Kapsokalyvas, D., Loos, J., Boogers, I.A.L.A., Appeldoorn, M.M., Kabel, M.A., Van Zandvoort, M., 2020. Quantification of morphochemical changes during in situ enzymatic hydrolysis of individual biomass particles based on autofluorescence imaging. Biopolymers 111, e23347. https://doi.org/10.1002/bip.23347

Kapsokalyvas, D., Wilbers, A., Boogers, I.A.L.A., Appeldoorn, M.M., Kabel, M.A., Loos, J., Van Zandvoort, M.A.M.J., 2018. Biomass Pretreatment and Enzymatic Hydrolysis Dynamics Analysis Based on Particle Size Imaging. Microscopy Microanal. 24, 517-525. https://doi.org/10.1017/S1431927618015143

Karp, E.M., Donohoe, B.S., O'Brien, M.H., Ciesielski, P.N., Mittal, A., Biddy, M.J., Beckham, G.T., 2014. Alkaline Pretreatment of Corn Stover: Bench-Scale Fractionation and Stream Characterization. ACS Sus. Chem. Eng. 2, 1481-1491. https://doi.org/10.1021/sc500126u

Lacey, J.A., Aston, J.E., Westover, T.L., Cherry, R.S., Thompson, D.N., 2015. Removal of introduced inorganic content from chipped forest residues via air classification. Fuel 160, 265-273. https://doi.org/10.1016/j.fuel.2015.07.100

Liao, K., Han, L., Yang, Z., Huang, Y., Du, S., Lyu, Q., Shi, Z., Shi, S., 2022. A novel in-situ quantitative profiling approach for visualizing changes in lignin and cellulose by stained micrographs. Carb. Polym. 297, 119997. https://doi.org/10.1016/j.carbpol.2022.119997

Liu, W., Wang, B., Hou, Q., Chen, W., Wu, M., 2016. Effects of fibrillation on the wood fibers' enzymatic hydrolysis enhanced by mechanical refining. Biores. Technol. 206, 99-103. https://doi.org/10.1016/j.biortech.2016.01.074

Mavridou, E., Vrochidou, E., Papakostas, G.A., Pachidis, T., Kaburlasos, V.G., 2019. Machine Vision Systems in Precision Agriculture for Crop Farming. J. Imaging 5. https://doi.org/10.3390/jimaging5120089

Mooney, C.A., Mansfield, S.D., Beatson, R.P., Saddler, J.N., 1999. The effect of fiber characteristics on hydrolysis and cellulase accessibility to softwood substrates. Enzyme Microbial Technol. 25, 644-650. https://doi.org/10.1016/S0141-0229(99)00098-8

Murtagh, F., Qiao, X., Crookes, D., Walsh, P., Basheer, P.A.M., Long, A., Starck, J.-L., 2005. A machine vision approach to the grading of crushed aggregate. Mach. Vision Appl. 16, 229-235. https://doi.org/10.1007/s00138-005-0176-7

Nickisch, H., Rasmussen, C.E., 2008. Approximations for Binary Gaussian Process Classification. J. Mach. Learning Res. 9, 2035-2078. https://www.jmlr.org/papers/volume9/nickisch08a/nickisch08a.pdf

Patel, K.K., Kar, A., Jha, S.N., Khan, M.A., 2012. Machine vision system: a tool for quality inspection of food and agricultural products. J. Food Sci. Technol. 49, 123-141. https://doi.org/10.1007/s13197-011-0321-4

Pedregosa, F., Varoquaux, G., Gramfort, A., Michel, V., Thirion, B., Grisel, O., Blondel, M., Prettenhofer, P., Weiss, R., Dubourg, V., others, 2011. Scikit-learn: Machine learning in Python. J. Mach. Learning Res. 12, 2825-2830. https://www.jmlr.org/papers/volume12/pedregosa11a/pedregosa11a.pdf?ref=https://githubhelp.com

Popovich, A., Sufiiarov, V., 2016. Metal powder additive manufacturing, in: Shishkovsky, I.V. (Ed.), New trends in 3D printing. IntechOpen. https://www.intechopen.com/chapters/50676

Ramos, L.P., Nazhad, M.M., Saddler, J.N., 1993. Effect of enzymatic hydrolysis on the morphology and fine structure of pretreated cellulosic residues. Enzyme Microbial Technol 15, 821-831. https://doi.org/10.1016/0141-0229(93)90093-H

Schindelin, J., Arganda-Carreras, I., Frise, E., Kaynig, V., Longair, M., Pietzsch, T., … Cardona, A. (2012). Fiji: an open-source platform for biological-image analysis. Nature Methods, 7, 676–682. https://doi.org/10.1038/nmeth.2019

Sluiter, A., Hames, B., Ruiz, R., Scarlata, C., Sluiter, J., Templeton, D., Crocker, D, 2012. Determination of Structural Carbohydrates and Lignin in Biomass. National Renewable Energy Laboratory Technical Report NREL/TP-510-42618. National Renewable Energy Laboratory, Golden, CO.

Sluiter, J.B., Sluiter, A.D., 2011. Laboratory Analytical Procedure (LAP) Review and Integration. National Renewable Energy Laboratory Technical Report NREL/TP-510-48087. National Renewable Energy Laboratory, Golden, CO.

Stickel, J.J., Adhikari, B., Sievers, D.A., Pellegrino, J., 2018. Continuous enzymatic hydrolysis of lignocellulosic biomass in a membrane-reactor system. J. Chem. Technol Biotechnol. 93, 2181-2190. https://doi.org/10.1002/jctb.5559

Templeton, D.W., Sluiter, A.D., Hayward, T.K., Hames, B.R., Thomas, S.R., 2009. Assessing corn stover composition and sources of variability via NIRS. Cellulose 16, 621-639. https://doi.org/10.1007/s10570-009-9325-x

Thompson, V.S., Lacey, J.A., Hartley, D., Jindra, M.A., Aston, J.E., Thompson, D.N., 2016. Application of air classification and formulation to manage feedstock cost, quality and availability for bioenergy. Fuel 180, 497-505. https://doi.org/10.1016/j.fuel.2016.04.040

Viamajala, S., McMillan, J.D., Schell, D.J., Elander, R.T., 2009. Rheology of corn stover slurries at high solids concentrations – Effects of saccharification and particle size. Bioresour. Technol. 100, 925-934. https://doi.org/10.1016/j.biortech.2008.06.070

Williams, D.L., Crowe, J.D., Ong, R.G., Hodge, D.B., 2017. Water sorption in pretreated grasses as a predictor of enzymatic hydrolysis yields. Bioresour. Technol. 245, 242-249. https://doi.org/10.1016/j.biortech.2017.08.200

Williams, D.L., Hodge, D.B., 2014. Impacts of delignification and hot water pretreatment on the water induced cell wall swelling behavior of grasses and its relation to cellulolytic enzyme hydrolysis and binding. Cellulose 21, 221-235. https://doi.org/10.1007/s10570-013-0149-3

Yan, J., Oyedeji, O., Leal, J.H., Donohoe, B.S., Semelsberger, T.A., Li, C., Hoover, A.N., Webb, E., Bose, E.A., Zeng, Y., Williams, C.L., Schaller, K.D., Sun, N., Ray, A.E., Tanjore, D., 2020.

Characterizing Variability in Lignocellulosic Biomass: A Review. ACS Sus. Chem. Eng. 8, 8059-8085. https://doi.org/10.1021/acssuschemeng.9b06263

Yang, L., Ru, Y., Xu, S., Liu, T., Tan, L., 2021. Features correlated to improved enzymatic digestibility of corn stover subjected to alkaline hydrogen peroxide pretreatment. Bioresour. Technol. 325, 124688. https://doi.org/10.1016/j.biortech.2021.124688

Zeng, M., Mosier, N.S., Huang, C.-P., Sherman, D.M., Ladisch, M.R., 2007. Microscopic examination of changes of plant cell structure in corn stover due to hot water pretreatment and enzymatic hydrolysis. Biotechnol. Bioeng. 97, 265-278. https://doi.org/10.1002/bit.21298

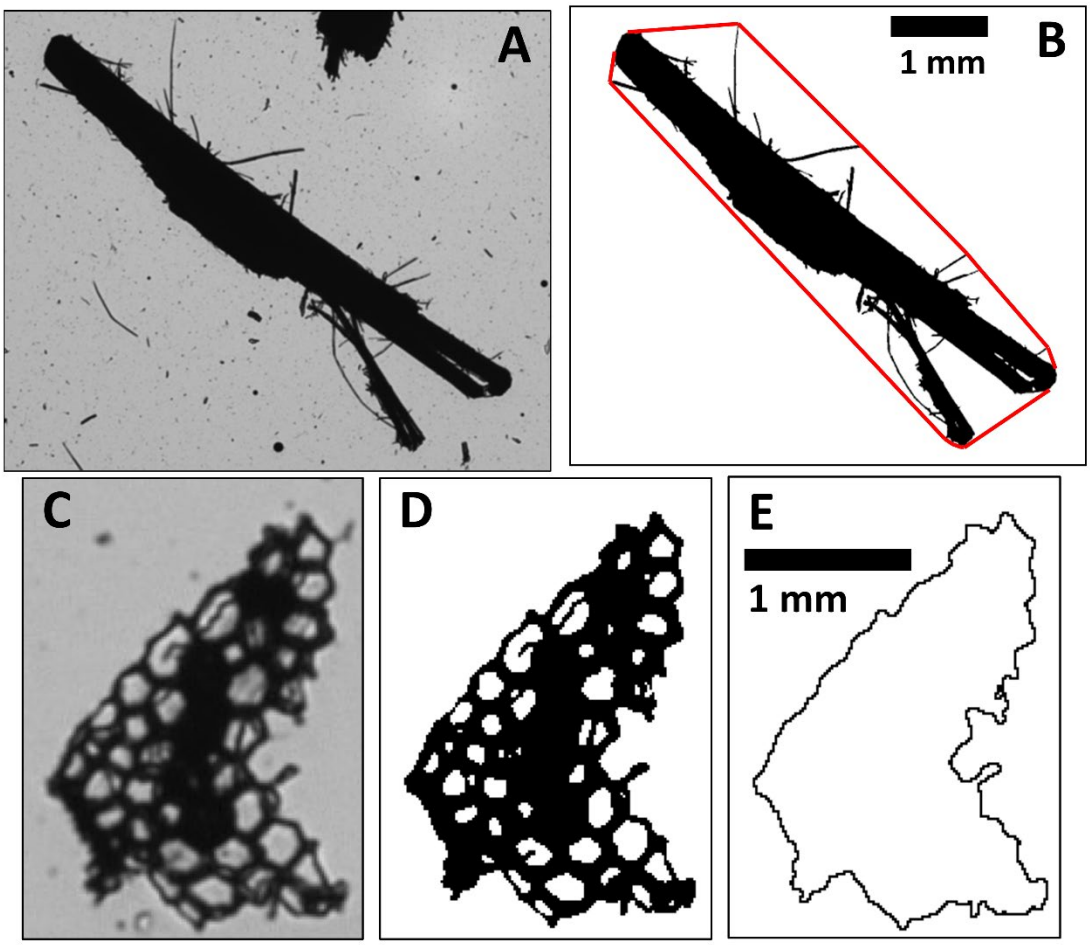
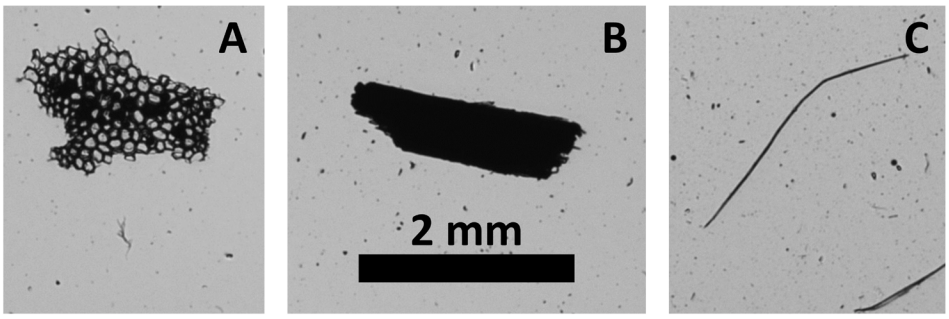


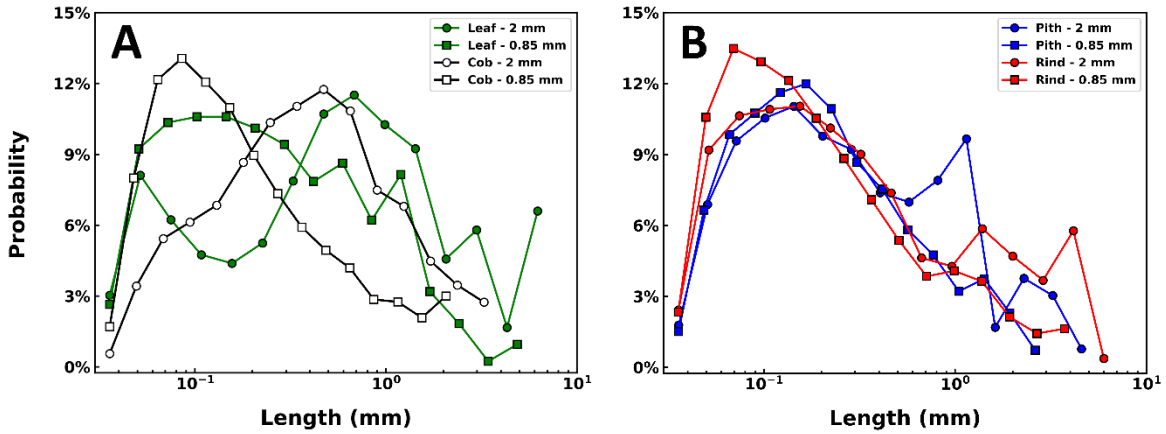
Figure 1. Demonstration of particle solidity calculation: the particle image (A) is binarized (B). The solidity is the total area interior to the red convex hull diameter in (B), divided by the black area of the particle. In the case of this bundle particle, the solidity is 0.483. Demonstration of %Area calculation: the particle image (C) is binarized (D) and the %Area is taken as the area of black space (B) enclosed by the perimeter (E) divided by the total space enclosed by the perimeter. In the case of this parenchyma particle from raw stalk pith, %Area = 79.3%.

667



668

669 **Figure 2**. Pith parenchyma (A), rind bundle (B), and rind fiber (C).



670

671 **Figure 3**. Area-weighted length distributions of (A) cob and leaf and (B) stalk components, pith, and rind
672 milled to two different screen sizes. N_{bins} = 15.

673

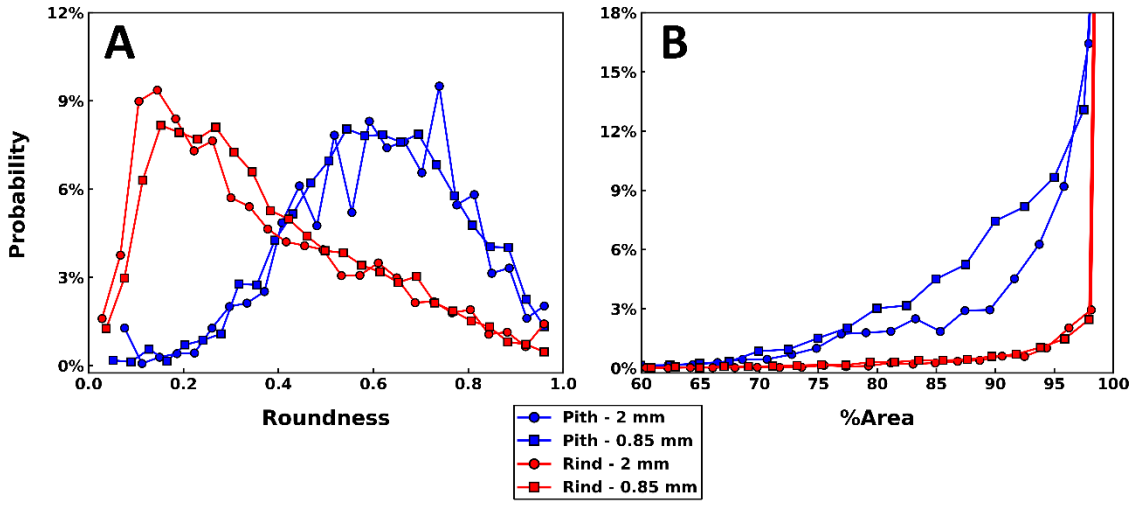


Figure 4. Area-weighted probability distribution of roundness (A) and area-weighted probability distribution of %Area (B) of anatomically pure stalk components, pith and rind, milled to pass two different screen sizes. $N_{bins} = 25$.

680

Particle Type	Bundle	Parenchyma	Fiber
Area	0.33	-0.075	-0.25
Perimeter	0.27	-0.18	-0.094
Width	0.31	-0.18	-0.12
Height	0.23	-0.25	0.028
Major	0.38	-0.31	-0.069
Minor	0.34	0.31	-0.66
Circularity	0.38	0.31	-0.70
Feret	0.29	-0.32	0.029
Minimum Feret	0.29	0.22	-0.51
Aspect Ratio	-0.18	-0.51	0.69
Roundness	-0.033	0.71	-0.67
Solidity	0.43	0.25	-0.68
%Area	0.33	-0.65	0.32

681

682 **Figure 5**. Pearson correlation coefficients of particle properties and particle type (bundle, parenchyma,
683 fiber). Green shading indicates positive correlation while red indicates a negative correlation. Darker
684 shading corresponds to stronger correlation.

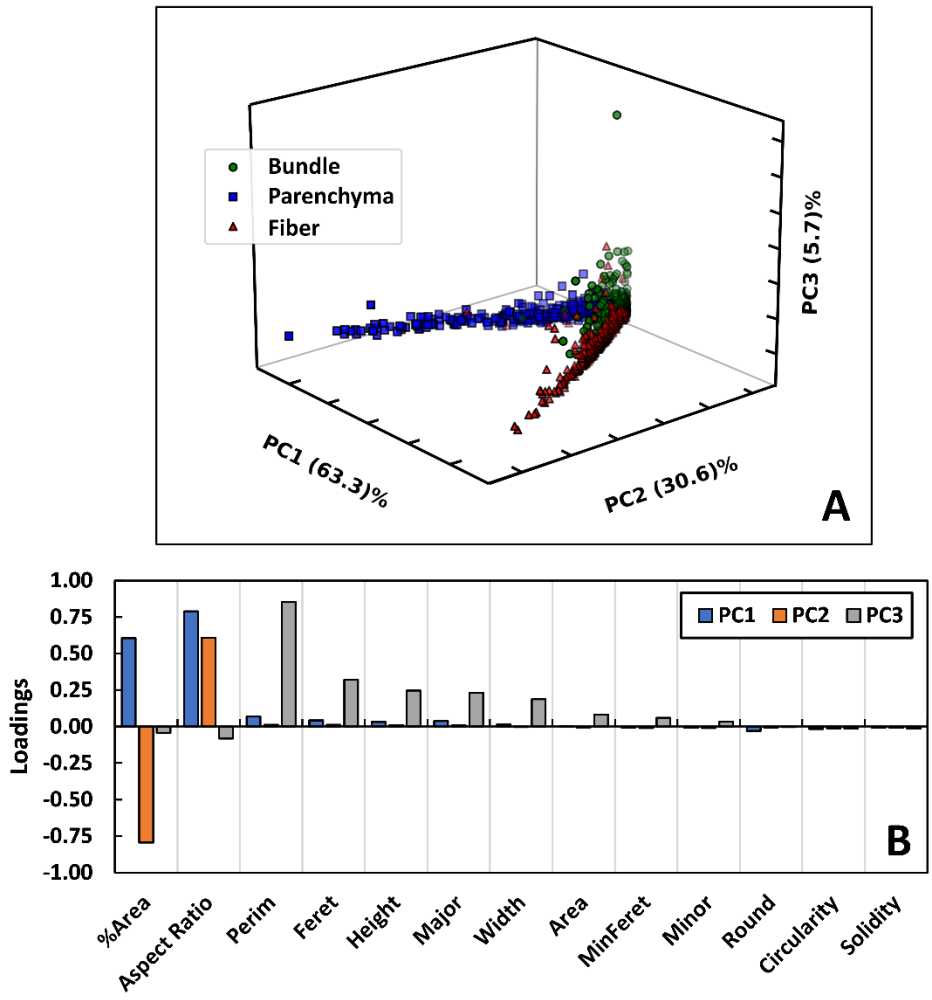


Figure 6. (**A**) The first three principal components of the particle characteristics for the 1380 manually classified particles and (**B**) loadings of particle characteristics for each of the first three principal components.

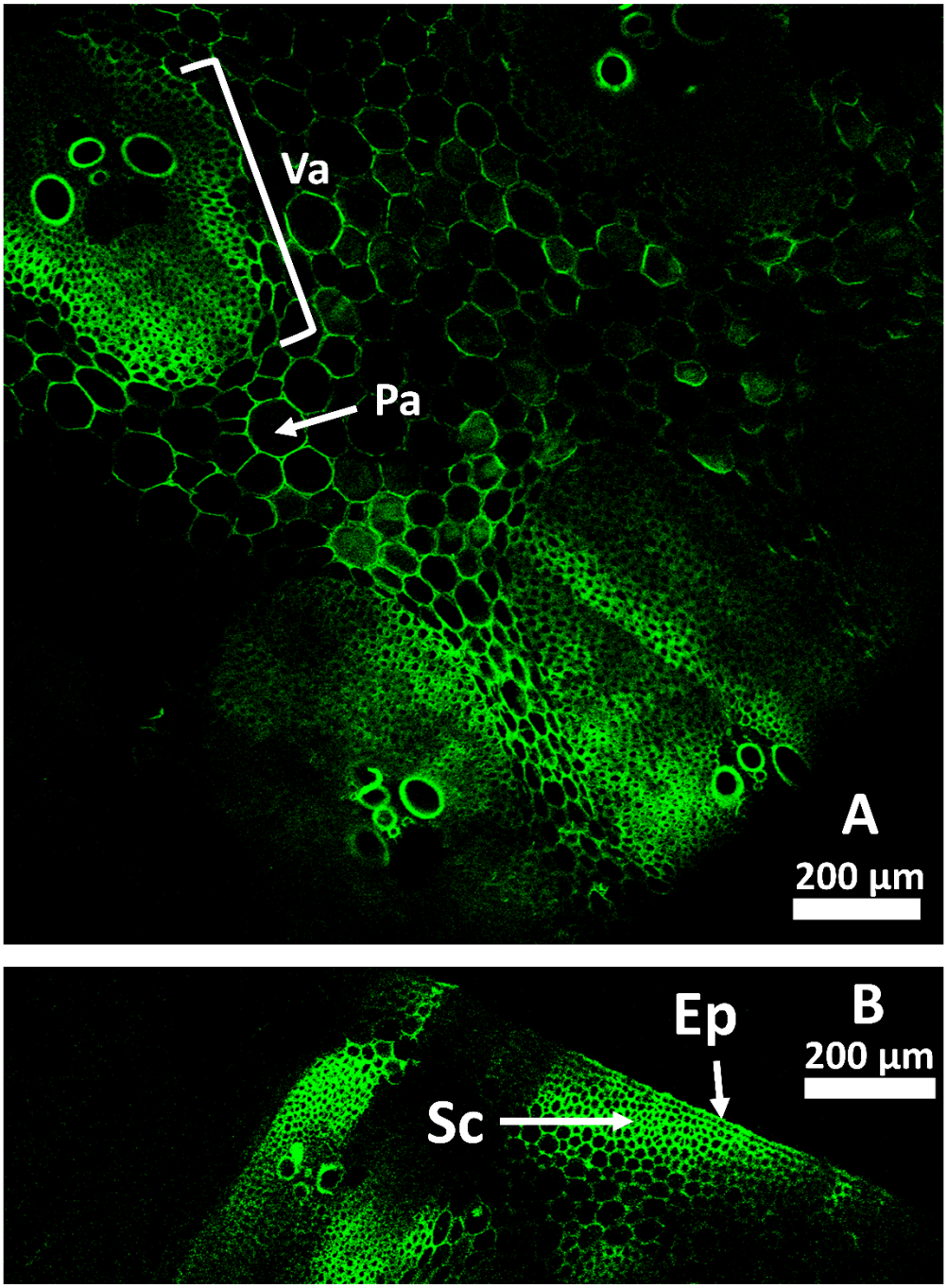
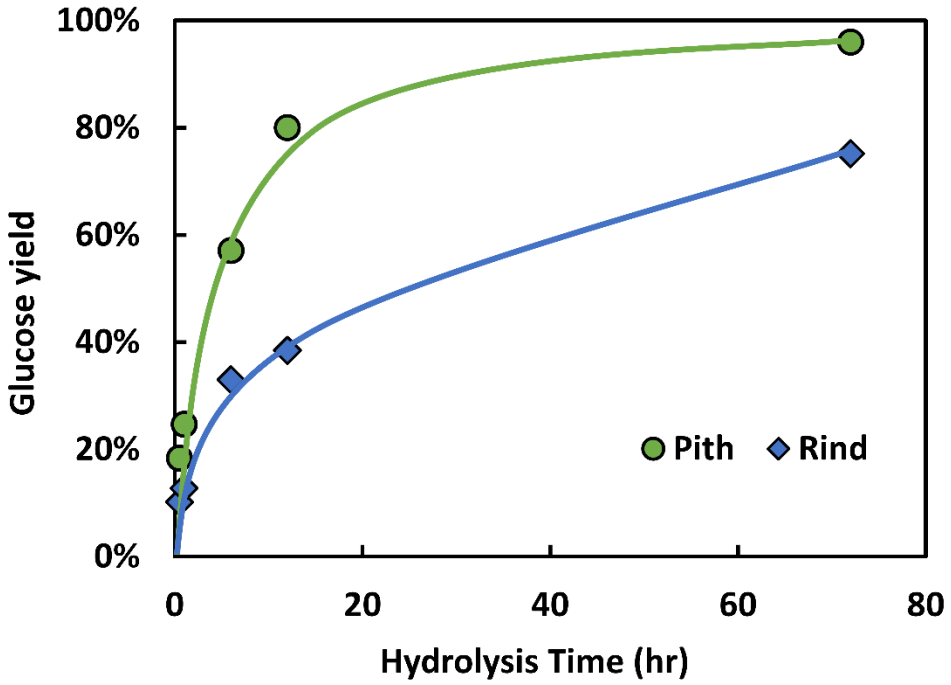


Figure 7. Confocal micrographs (**A**) near the middle of the stalk and (**B**) at the edge of the stalk. Green intensity corresponds to lignin autofluorescence. Annotations of cell types: Pa – parenchyma, Sc – sclerenchyma, Ep – epidermis, Va – vascular bundle.



692 **Figure 2**.
693 Glucose yields from progressive enzymatic hydrolysis of alkaline pretreated of stalk pith and rind. Lines
694 are presented to guide the eye.

695

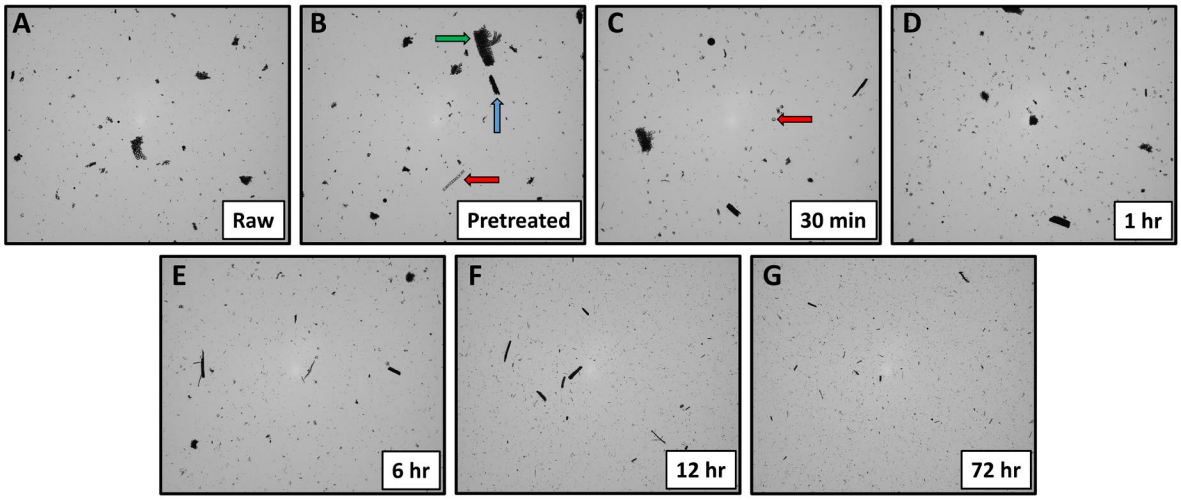


Figure 9. Selected images from the particle analyzer covering pretreatment and enzymatic hydrolysis of stalk pith. Parenchyma particles are observed to disintegrate within 12 hr of enzymatic hydrolysis and nearly all particles are disintegrated after 72 hr. Enzymatic hydrolysis was carried out on the pretreated material.

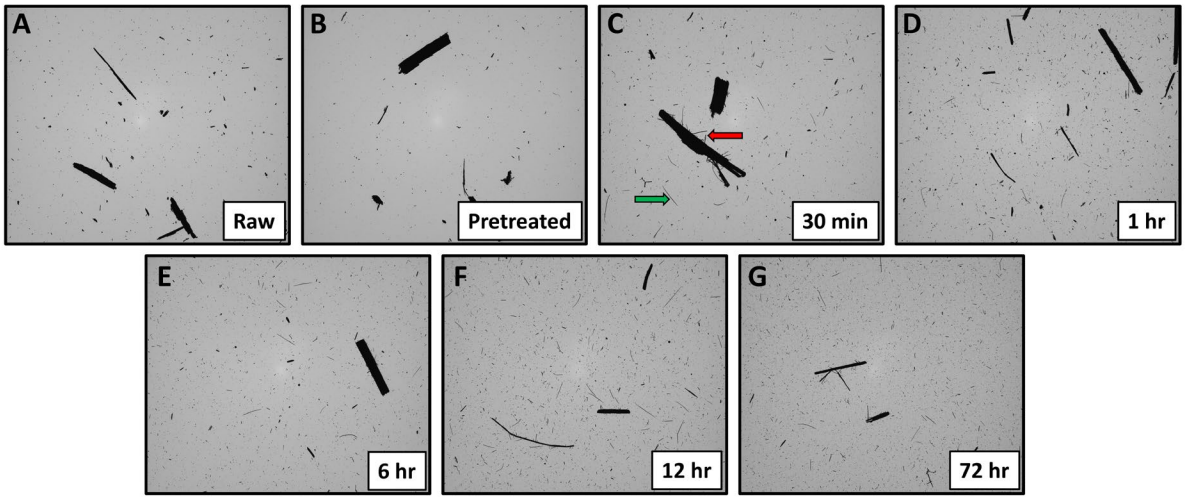


Figure 10. Selected images from the particle analyzer covering pretreatment and enzymatic hydrolysis of stalk rind. Enzymatic hydrolysis was carried out on the pretreated material.

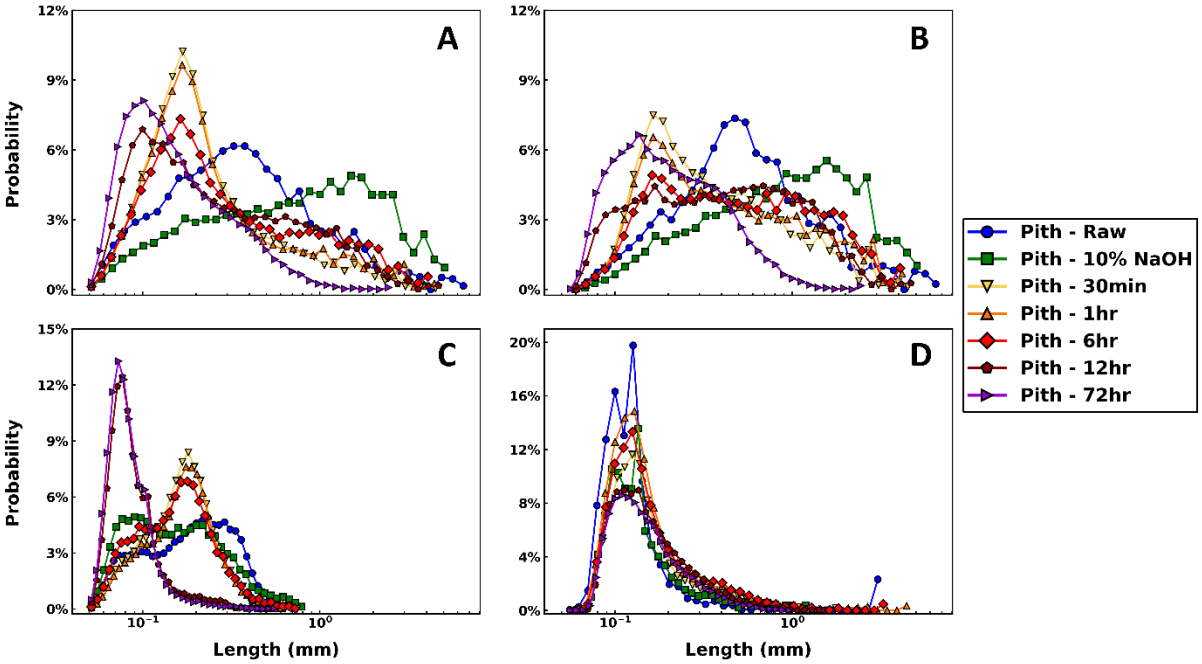


Figure 11. Area-weighted particle length probability distributions of stalk pith as a function of pretreatment and enzymatic hydrolysis time for (A) all particles, (B) bundles, (C) parenchyma, and (D) fibers. Enzymatic hydrolysis was carried out on the pretreated material. N_{bins} = 35.

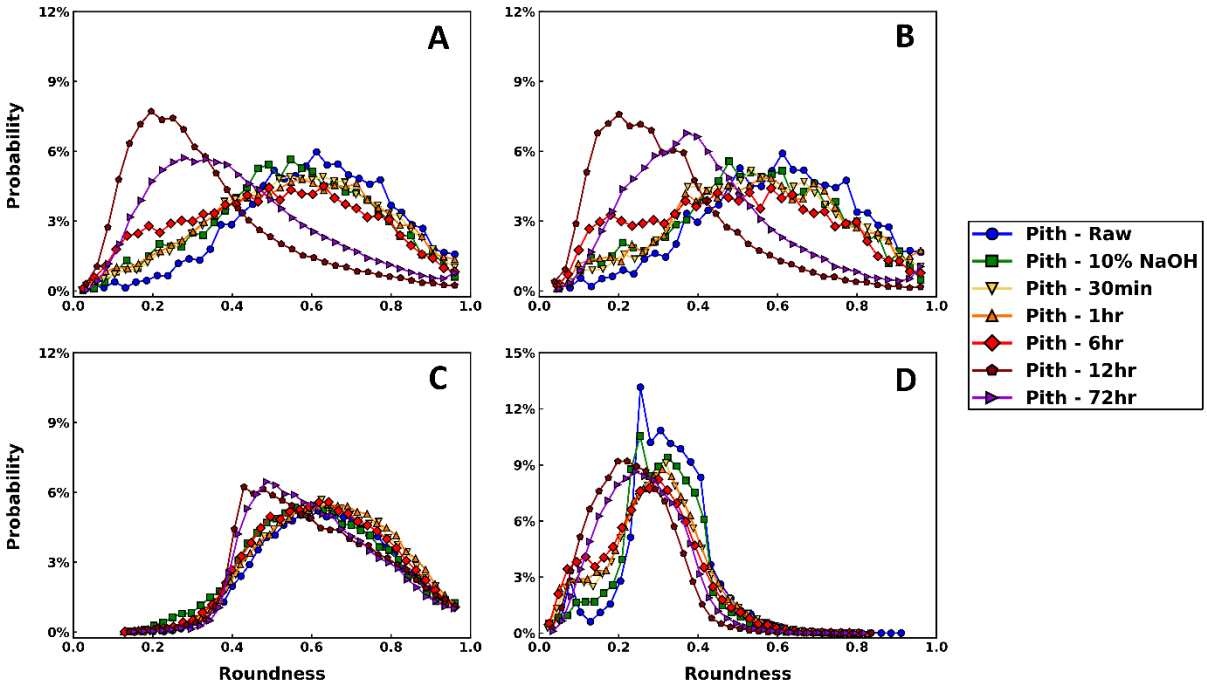


Figure 12. Area-weighted particle roundness (inverse of aspect ratio) probability distributions of stalk pith as a function of pretreatment and enzymatic hydrolysis time for (A) all particles, (B) bundles, (C) parenchyma, and (D) fibers. Enzymatic hydrolysis was carried out on the pretreated material. N_{bins} = 35.

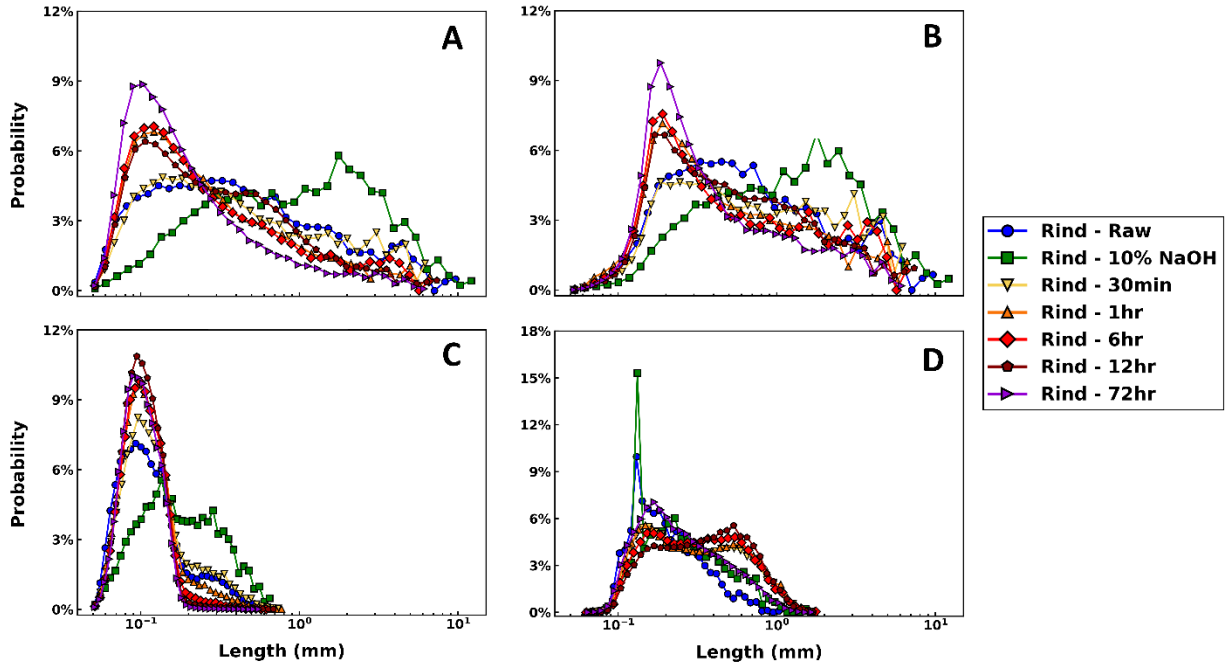


Figure 13. Area-weighted particle length probability distributions of stalk rind as a function of pretreatment and enzymatic hydrolysis time for (A) all particles, (B) bundles, (C) parenchyma, and (D) fibers. Enzymatic hydrolysis was carried out on the pretreated material. N_{bins} = 35.

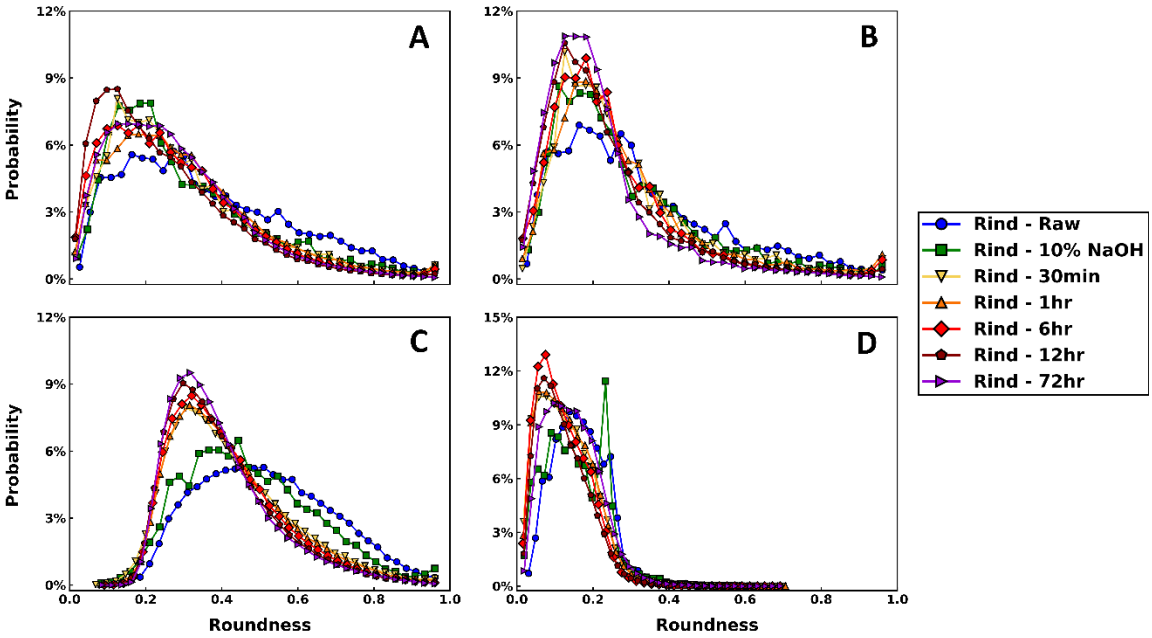


Figure 14. Area-weighted particle roundness (inverse of aspect ratio) probability distributions of stalk rind as a function of pretreatment and enzymatic hydrolysis time for (A) all particles, (B) bundles, (C) parenchyma, and (D) fibers. Enzymatic hydrolysis was carried out on the pretreated material. N_{bins} = 35.

732 **Table 1**. Accuracy (correct classification/total classifications) for various classification algorithms to
733 predict particle type (bundle, parenchyma, or fiber) over 30 model runs.

Classifier	Average Accuracy	Standard Deviation
Nearest Neighbors	93.3%	1.7%
Linear SVM	93.5%	1.7%
RBF SVM	90.9%	2.1%
Gaussian Process	96.4%	1.3%
Decision Tree	94.1%	2.3%
Random Forest	93.4%	2.1%
Neural Network	95.7%	1.6%
Adaptive Boosting	90.5%	3.6%
Naïve Bayes	81.6%	2.5%
QDA	84.8%	1.9%

734